Computational Fluid Dynamics Conference at AVIATION Forum, 17 - 21 June 2019, Dallas, USA

Hybrid RANS/LES Simulation of Vortex Breakdown Over a Delta Wing

Beckett Y. Zhou* and Nicolas R. Gauger†

Chair for Scientific Computing, TU Kaiserslautern

Bldg 34, Paul-Ehrlich-Strasse, 67663 Kaiserslautern, Germany

Christos Tsolakis‡ Juliette Pardue§

Andrey Chernikov¶ Fotis Drakopoulos‖ and Nikos Chrisochoides**

Department of Computer Science, Center for Real-Time Computing, Old Dominion University

5115 Hampton Blvd Norfolk, VA 23529, USA

Boris Diskin††

National Institute of Aerospace

100 Exploration Way, Hampton, VA 23666, USA

Hybrid RANS-LES computations are performed for the turbulent flow around a delta wing at a low subsonic Mach number $M_\infty = 0.07$ and an angle of attack of $23°$. An automated mesh generation methodology is used to generate a mixed-element mesh around the delta wing with a sharp leading edge and a leading-edge sweep angle of $65°$. The delayed detached eddy simulation with shear-layer adapted (SLA) subgrid scale model in the SU2 open-source solver suite has been applied to predict the vortex breakdown phenomenon that is known to occur at these flow conditions. Three meshes of increasing density are considered. Mean pressure distribution, resolved turbulence kinetic energy and mean axial velocity distribution obtained from the simulations are compared with experimental data. It is clear from current results that a fine mesh adapted to the essential flow physics in leading edge and the vortex core regions is necessary to better capture the shear layer instability and vortex breakdown phenomenon.

I. Introduction

Delta wings are typically employed in high-performance aircraft that require high agility and maneuverability and have been studied extensively both experimentally[1–3] and numerically[4,5] in the past. At supersonic speeds, delta wings with highly swept sharp leading edges are aerodynamically more efficient than the conventional high-aspect-ratio wings due to its low supersonic wave drag. Lift generation mechanism of a delta wing is fundamentally different from that of a conventional slender wing. The lift force on a delta wing is largely determined by the suction due to the vortices above the wing.[6] Up to a moderate angle of attack ($\alpha < 20°$), the shear-layers emanating from the wing leading edges roll up, starting immediately at the apex forming a distinctive vortex system above the wing. These vortices result in strong suction peaks near the leading edges inboard which correspond to significantly reduced static pressure within the vortex cores, which in turn leads to increased lift. As the angle of attack increases, the vortices become stronger and the lift is enhanced. At a sufficiently high angle of attack, large adverse pressure gradient causes

*Research Scholar, Member AIAA, yuxiang.zhou@nianet.org

†Professor, Associate Fellow AIAA, nicolas.gauger@scicomp.uni-kl.de

‡Co-first Author, Research Scholar, Member AIAA, ctsolakis@cs.odu.edu

§Research Scholar, Member AIAA, jpardue@cs.odu.edu

¶Associate Professor, achernik@cs.odu.edu

‖Research Scholar, fdrakopo@gmail.com

**Professor, nikos@cs.odu.edu

††Research Fellow, Associate Fellow AIAA, boris.diskin@nianet.org

the vortices to break down, the suction effect is then lost, and the lift drops strongly. In addition, the vortex breakdown and its interaction with the airframe lead to a number of undesirable aeromechanical effects. The impingement of the turbulent wake on the vertical stabilizer of the aircraft causes strong vibrations and structural fatigue. The asymmetry at the onset of the vortex breakdown also triggers instability about the roll axis. Therefore, to reliably design and control the delta wing aircraft, it is of paramount importance to accurately predict the strength and location of vortex breakdown as well as the flow conditions at which breakdown occurs.

From the simulation perspective, such highly nonlinear, unsteady turbulent flow places strong demands on computational fluid dynamic (CFD) solvers. To accurately simulate this flow, it is not only essential to capture the shear layer roll-up from the leading edge, but the ensuing Kelvin-Helmholtz instability in the free shear layer must be also be allowed to develop rapidly, as the vortex breakdown process is known to be highly sensitive to such instabilities. To that end, unsteady Reynolds-averaged Navier-Stokes (URANS) approaches, which are still the workhorse of the aircraft industry, have shown limited success in predicting massively separated turbulent flows.[7] Large-eddy simulation (LES) seems to be a more suitable approach for such flows, but is still prohibitively expensive when considering high-Reynolds number wall bounded flows. Therefore, in this work we opt for a more practical alternative – the hybrid RANS/LES approach, where the solver operates in RANS mode in the attached boundary layer thus relaxing the grid resolution requirements close to walls and switches to a low dissipation LES mode in the separated region. In particular, the delayed detached eddy simulation (DDES)[8] based on the Spalart-Allmaras turbulence model[9] is used.

A well known difficulty concerning the DDES-type approaches is the unphysically slow development of resolved turbulence as the method switches from RANS to LES. In particular, the development of Kelvin-Helmholtz instabilities in free shear layers separating from the delta wing leading edge, may be significantly delayed. In this work, we use a new sub-grid scale (SGS) proposed by Shur et al., known as the shear-layer adapted (SLA) SGS.[10] This SGS employs a vorticity-sensitive ‘vortex tiling measure’, aimed at unlocking the Kelvin-Helmholtz instability in the initial part of the shear layer, thus inducing a more rapid development of shear-layer instabilities and full three-dimensional turbulence.

From the mesh generation perspective, sufficient mesh resolution needs to be placed around the leading edge where the shear layers roll-up occur. In addition, the mesh must be progressively refined in the regions where the important flow physics take place. In the case of a delta wing experiencing vortex breakdown, this corresponds to the vortex core where the fine-scaled, three-dimensional turbulence structures develop in the post-breakdown region of the vortex core. Therefore, adaptive mesh refinement (AMR) techniques should be applied to these ‘focus regions’ where the turbulent wake impart unsteady loads on vertical stabilizers of more realistic delta wing configurations. Pirzadeh[11] showed the numerical prediction of these vortical flows was highly sensitive to the local grid resolution and that grid adaptation is essential to the application of CFD to these flows. In particular, the grid-adapted solutions were shown to be far more superior in capturing the vortical flow structure over the conventional unadapted results by comparisons with wind-tunnel data.

The proposed mesh generation method is based on two building blocks targeting two different regions of the input geometry. A Boundary Layer (BL) approach [12] for the viscous region and a parallel local reconnection method[17] for the inviscid region. The BL approach uses multiple normals at nodes to maintain the alignment and orthogonality of the anisotropic volume elements with respect to the surface. The NASA CFD Vision 2030 Study[13] has identified that mesh generation is a significant bottleneck in the CFD workflow because mesh generation routinely requires human intervention due to a lack of robustness in treating complex geometries. Another key finding is a lack of automation. To address this, the BL approach uses an exhaustive enumeration scheme to classify each node of the surface mesh where each classification has an associated meshing template. The BL approach is fully automated and capable of handling arbitrary geometries. The only required inputs are the surface mesh and the boundary layer growth function. The inviscid region mesh generator CDT3D is applied on the boundary generated by the BL method. CDT3D preserves boundary throughout the unstructured mesh generation process allowing the decoupling of the two grid generation methods. Vertex-spacing is derived from the boundary minimizing thus the number of extra user input. Recent advances in the CDT3D mesh generation code [22] will enable in the future parallel solution-based anisotropic grid adaptation.

In this work, we apply the aforementioned mesh generation and the DDES-SLA methodology to simulate the vortex breakdown over a delta wing. The remainder of the paper is organized as follows. In Section II, the mesh generation and the DDES-SLA simulation methodology are presented. Numerical results are presented in Section III while conclusion and outlook to future work are outlined in Section IV.

II. Mesh Generation and Simulation Methodology

A. Mesh Generation Methodology

1. Viscous Region Mesh generation

An automated approach to generating unstructured three-dimensional, prism-dominant meshes for viscous flows is used to generate the semi-structured boundary layer mesh.[12] An extrusion-based approach using multiple normals is used where anisotropic prisms are formed from the surface mesh facets and blend prisms are used to fill the cavities between multiple normals. Normals are chosen that satisfy the visibility requirement, the dot product between the node's chosen normal and an incident surface facet's calculated normal being above a threshold. When all of a node's incident surface facets satisfy the visibility requirement, then only one normal is needed for the node; otherwise, multiple normals are needed. However, when multiple normals are introduced, the cavity between these multiple normals has highly anisotropic faces exposed. These anisotropic faces are covered in a semi-structured manner similarly to how the remainder of the boundary layer is formed.

Prism-dominant meshes have been shown to have better accuracy than their purely-tetrahedral counterparts for simulations with viscous flows. Park and Anderson compared the convergence and accuracy of solutions computed from a finite-volume scheme on hexahedral meshes, a finite-element scheme on tetrahedral meshes, and a finite-volume scheme on tetrahedral meshes.[14] Varying mesh sizes were used and the largest tetrahedral mesh for the finite-volume scheme was not able to accurately resolve the same flow features as the smallest hexahedral mesh for the finite-volume scheme. The velocity profiles were also compared and the finite-volume scheme over hexahedral meshes and the finite-element scheme over tetrahedral meshes both agree with the reference solution. However, there is a large disparity in the velocity profile for the finite-volume scheme over tetrahedral meshes compared to the reference solution.

The first step for extruding a viscous boundary layer from the surface mesh is to analyze the surface mesh's edges. The angle at each edge is calculated as the angle between the two incident surface triangles' normals. Based on the winding of the triangles, it is determined if this edge causes a concavity or convexity. For convex edges, if this angle is above the user-defined threshold, 80 degrees for this case, then the edge is marked as a convex ridge. Multiple normals are needed at these convex ridges. Triangular prisms are extruded from the surface triangles. Prism-dominant blend meshes are extruded from the convex ridges.

The farfield domain is generated using two user-specified parameters: the farfield bounding box and the desired edge length metric at the farfield vertices. The farfield is generated using a right-triangular uniform tiling procedure. The symmetry plane and outflow plane are discretized using Shewchuk's Triangle.[16] The outer surface of the boundary layer and the farfield boundary are passed to the inviscid region tetrahedral mesh generator.

2. Inviscid Region Mesh generation

The mesh of the inviscid region is generated using CDT3D[17] . CDT3D implements a parallel method for topological transformations for local reconnection. This scheme combines known parallel techniques like data over-decomposition and load balancing [20] with widely used topological transformations also known as flips or swaps. In contrast to most mesh generation methods, the proposed scheme optimizes the connectivity in parallel throughout the mesh generation procedure. The speculative scheme is implemented with a tightly coupled approach[19] . CDT3D exploits fine-grain parallelism at the cavity level using data decomposition. Its current implementation targets shared memory multi-core nodes using multithreaded execution at the chip level.

The pipeline of CDT3D can be divided into three main steps, initial mesh construction, mesh refinement and (optionally) mesh quality optimization, see Figure 1. In the first stage, the triangulated surface mesh of the viscous

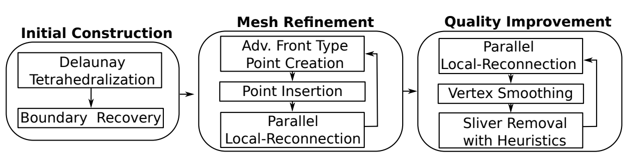

Figure 1. The CDT3D mesh generation pipeline.

region described in the previous section is recovered using methods based on Delaunay tetrahedralization. In practice, recovering the boundary is accomplished by creating a boundary conforming tetrahedral mesh i.e. all the faces of the input surface appear as a face of some tetrahedron. The robustness of boundary recovery implementation has been extensively evaluated and it has been found to be in-par with state-of-the-art boundary recovery methods [18] . For the current application this feature is crucial since introducing even a single point on the boundary of the viscous region mesh would require to modify the boundary layer mesh which is non-trivial.

Mesh refinement introduces points iteratively into the mesh using advancing front point creation and direct insertion. The advancing front method offers great control on point density and especially on the growth of the spacing between the generated points. The spacing of the points is initialized by the spacing (i.e. edge length) of the surface mesh. The growth of the size of the tetrahedra follows an exponential distribution with parameters controlled by the user. After each point creation iteration, the connectivity of the mesh is optimized in parallel using a fine-grained topological scheme for local reconnection [17] , optimizing metric-based criteria. For this paper a combined criterion of the Delaunay in-sphere criterion and the maximization of the minimum edge-weight [21] is used. The combined criterion is evaluated for every set of two(three) neighboring tetrahedra that a 2-3(3-2) flip can be applied. The configuration that improves the combined criterion is then used.

In the last stage, the mesh quality is improved using a combination of mesh smoothing, parallel local reconnection, and heuristics to target the improvement of low quality elements. Extensive evaluation of the effectiveness of the quality improvement step against state-of-the-art local reconnection methods can be found in [17] .

B. DDES-SLA Solver in SU2

The SU2 open source software suite[23] was specifically developed for solving problems governed by partial differential equations (PDEs) and PDE-constraned optimization problems. It was developed with the aerodynamic shape optimization problems in mind. Therefore the suite is centered around a RANS solver capable of simulating compressible, turbulent flows commonly found in problems in aerospace engineering. The governing equations are spatially discretized using the finite volume method, on unstructured meshes using a standard edge-based data structure on a dual grid with control volumes constructed using a median-dual, vertex-based scheme. A number of convective fluxes discretization schemes have been implemented, such as the Jameson-Schimdt-Turkel (JST) scheme and the upwind Roe scheme. The turbulence can be either modeled by the Spalart-Allmaras(SA) model or the Menter Shear Stress Transport (SST) model. For unsteady flows, a dual time-stepping method[24] can be used, leading to second-order accuracy in space and time.

Regarding scale-resolving capabilities, the delayed detached eddy simulation (DDES) method based on the SA turbulence model was implemented by Molina.[25] To overcome the known issue of slow transition from RANS to LES in the shear-layer, a shear-layer adapted (SLA) subgrid scale (SGS) proposed by Shur et al.[10] was used to replace the conventional DDES SGS. This new SGS does not only depend on the grid spacing in each spatial direction but also incorporates a solution-dependent indicator known as the ‘vortex tilting measure’. The VTM varies from 0.0 to 1.0, being close to zero in the quasi-2D regions of the flow where the vorticity vector an eigenvector of the strain, and near unity in the region of developed 3D turbulence. This leads to a significant reduction of the eddy viscosity in the initial region of the shear layer, thus unlocking the Kelvin-Helmholtz instability and allowing the development of 3D turbulent structures. In addition, the Simple Low-dissipation AUSM (SLAU2)[26] convective flux scheme was also implemented.

III. Results

A. Mesh Generation

1. Boundary Layer Mesh generation

For the Delta Wing model in Figure 2(a), blend regions will be extruded from the sharp edges between the marked triangles. Figure 2(b) shows the exposed blend cavities with the anisotropic quadrilateral faces of the Delta Wing after prisms have been extruded from the surface triangles. Fans of multiple normals are created at each node that has more than one normal so that the outer layer blend prisms have approximately the same volume as the neighboring outer layer triangular prisms that are extruded from the surface triangles incident upon the convex ridge. Figure 2(c) shows the added blend volume elements, triangular prisms stacked on top of the first layer pyramids and tetrahedra. Figure 3(a) shows the outer surface of the boundary layer along with the symmetry plane and outflow plane of the farfield boundary, and Figure 3(b) show the farfield bounding box.

2. *Inviscid Region Mesh generation*

For the inviscid region mesh generation, CDT3D was supplied with the external boundary of the boundary layer mesh (Figure 3). The surface of the boundary layer was kept fixed to achieve conformity while the rest of the surfaces were refined as needed. For the finer cases, a refinement zone will be used, to provide a semi-automatic adaptation based previous experimental data [2] . The refinement zone consists of three simple solids : a pyramid aligned to the upper surface of the wing and two hexahedra on the wake region see Figure 4. The size of the elements is initialized by the spacing on the surface of the boundary layer and it is limited to a constant size within the refinement. Outside of the refinement zones the element size follows a quadratic growth function based on the distance from the refinement zone boundary.

Finally, the meshes of the viscous and inviscid regions are merged along the frozen surface (see Figure 5), and passed to the solver.

B. SU2 DDES-SLA Simulation

The DDES-SLA method was used to simulate the turbulent flow over a delta wing with a sharp leading edge and a leading-edge sweep angle of 65°.[1] A freestream Mach number of $M_\infty = 0.07$, a Reynolds number of $Re_{MAC} = 1 \times 10^6$ based on the mean aerodynamic chord c_{mac} , and an angle of attack of $\alpha = 23°$ are considered. At these conditions, the delta wing experiences vortex breakdown over its upper surface. In experiment, the vortex breakdown is observed between $x/c_r = 0.60$ and $x/c_r = 0.80$. Three meshes of increasing densities are considered for this study (Table 1). Second-order dual time stepping method is used for time marching, with a nondimensional time step of 3.5×10^{-4}. The turbulent flow statistics are computed over a period of 15 convective time units (CTU), after an initial transient of 10 CTU.

In Figure 6, instantaneous vortical structures are visualized by iso-surfaces of Q criterion colored by vorticity magnitude. It is clear that the coarse mesh is too dissipative where the main vortex core is hardly visible. For the medium mesh, the shear layer roll-up along the leading edges as well as the large helical structures over the suction side of the wing are clearly visible. The fine mesh shows in addition, more fine-scale turbulent structures along the leading edge of the wing. While the solver has been able to capture the large structures, it does not appear to capture the shear layer instability which is critical to accurate prediction of vortex breakdown.

Figure 7 compares the mean spanwise pressure coefficient at 5 different chordwise stations over the wing against experimental data as well as numerical results obtained using X-LES with a high-pass filtered SGS model and a stochastic backscatter model provided by J. Kok of NLR.[29] At the first station ($x/c_r = 0.20$), all numerical results predict a pronounced main suction peak which is not present in the experimental result. Evidently, in the experiment, a clear detached vortex has not yet formed at a station so close to the apex of the wing. It should also be noted that current results from all three meshes show a secondary suction peak to various levels outboard of the main vortex – an evidence that they all falsely predict the secondary separation at this station. The NRL result however, shows a pressure plateau in that region, which more closely resembles the experimental data. At the second station ($x/c_r = 0.40$), the fine mesh completely misses the main suction peak. On the other hand, the medium mesh is in better agreement with the experiment. At all other stations further downstream, the fine mesh result is in good agreement with both the experiment and the NLR result. In particular, the level of the mean C_p at the suction peak below the main vortex is higher and in closer agreement with experiment compared to the two coarser meshes.

Figure 8 compares the levels of resolved turbulence kinetic energy (TKE) from the medium and fine meshes against the measured TKE from hotwire measurement at three chordwise stations. The resolved TKE level of the

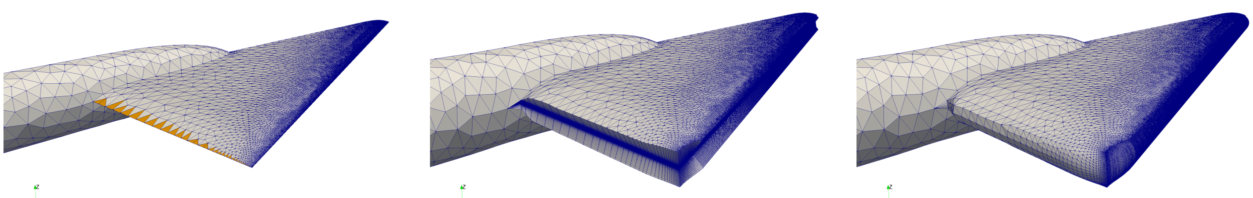

(a) Delta wing surface with convex ridge triangles marked

(b) Extruded triangular prisms

(c) After exposed quadrilateral faces have been covered

Figure 2. The Delta Wing surface and exposed anisotropic quadrilateral faces in the blend region after the triangular prisms have been extruded. The final image shows the blend mesh added along the ridge cavities.

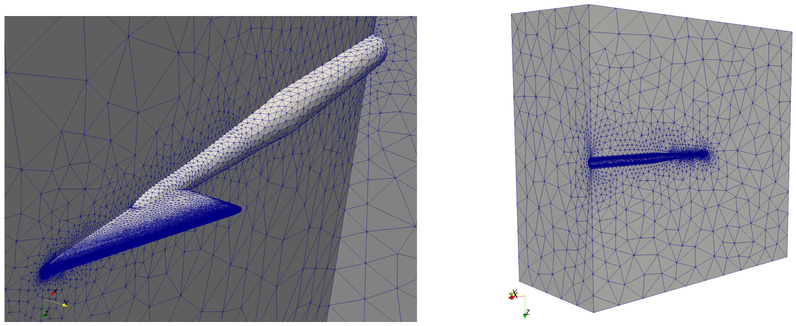

(a) Outer surface of the boundary Layer inside the farfield boundary

(b) Farfield bounding box with symmetry plane and outflow plane

Figure 3. Farfield Domain

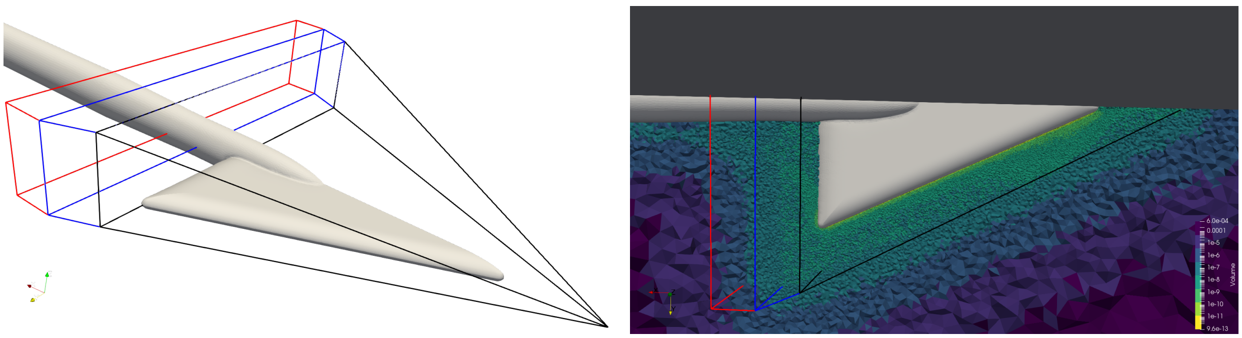

(a) Refinement zones of the inviscid region.

(b) Generated inviscid region mesh.

Figure 4. Refinement zones and their effect on the final fine mesh.

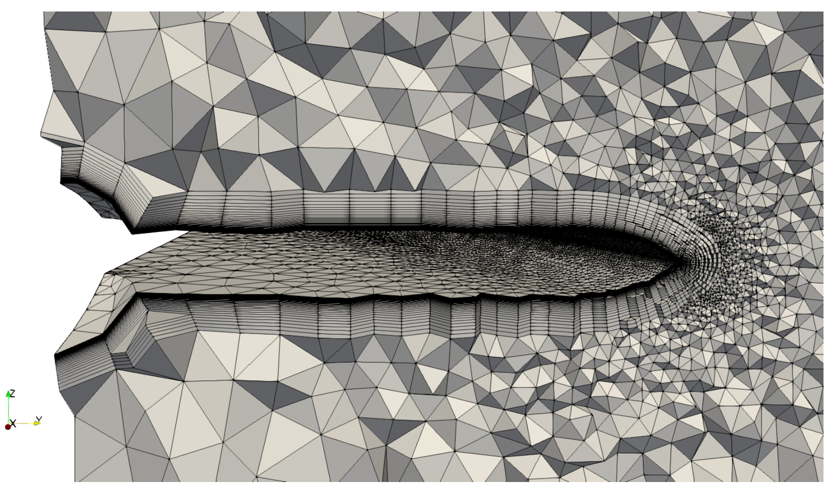

Figure 5. Viscous and inviscid meshes combined. Mesh cut at $x/c = 0.7$

coarse mesh is three orders of magnitude below the lower limit of the scale in this comparison and is therefore not shown here. At the station $x/c_r = 0.40$, the fine mesh shows the resolved turbulence has started to develop near the tip region but under-predicts its size. The medium mesh on the other hand, shows practically no resolved turbulence. It is therefore surprising to see that at $x/c_r = 0.60$ just before the vortex breakdown, the medium mesh shows a significantly higher level of resolved turbulence compared to both the hotwire measurement and the fine mesh. Post-breakdown ($x/c_r = 0.80$), both the level and distribution of resolved turbulence from the fine mesh appear to be in good agreement with the measurement.

The time-averaged axial velocity distribution of the three meshes are compared to the hotwire measurements in Figure 9. Both the coarse and medium meshes predict vortex breakdown already at $x/c_r = 0.60$. The medium mesh result in particular, shows a clear low-velocity region in the vortex core, which appears to be in agreement with the hotwire measurements. However, it should be noted that the hotwire measurements are intrusive and have likely triggered an early vortex breakdown. In fact, in a more recent measurement conducted using the non-intrusive particle image velocimetry (PIV) technique,[29] the vortex breakdown is shown to take place between $x/c_r = 0.60$ and $x/c_r = 0.80$. Therefore, the fine mesh results indeed predict the location of the vortex breakdown correctly.

Mesh	Number of Elements	Number of Points
Coarse	4,269,010	1,651,540
Medium	15,912,583	6,073,907
Fine	61,595,969	23,492,665

Table 1. Meshes of three levels of refinement used in this study

IV. Conclusion

In this paper, the mesh generation and scale-resolving simulation capabilities necessary for turbulent flow prediction over a delta wing configuration are demonstrated. In particular, the automated mesh generation methodology outlined in Section II has been used to generate a mixed-element mesh around a delta wing. The DDES-SLA solver in the SU2 suite has been applied to predict the turbulent flow over a delta wing with a leading edge sweep angle of 65° experiencing vortex breakdown at an angle of attack of 23°. Mean pressure distribution, resolved turbulence kinetic energy and mean axial velocity distribution obtained from the simulations are compared with experimental data. It is clear from current results that a fine mesh adapted to the essential flow physics in leading edge and the vortex core regions is necessary to capture the shear layer instability and vortex breakdown phenomenon.

V. Acknowledgement

The authors would like to gratefully acknowledge Mike Park of the NASA Langley Research Center for his insightful suggestions during numerous discussions. The authors would also like to thank Johan Kok of the Netherlands Aerospace Center (NLR) for providing the X-LES results for comparison. In addition, the computational resources provided by the RHRK high performance computing center via the Elwetritsch high performance cluster at the TU Kaiserslautern is gratefully acknowledged. This research for Mr. Tsolakis and Prof. Chrisochoides was sponsored in part by NASA's Transformational Tools and Technologies Project (grant no. NNX15AU39A) of the Transformative Aeronautics Concepts Program under the Aeronautics Research Mission Directorate, NSF grant no. CCF-1439079, ODU Modeling and Simulation Fellowship and Richard T. Cheng Endowment.

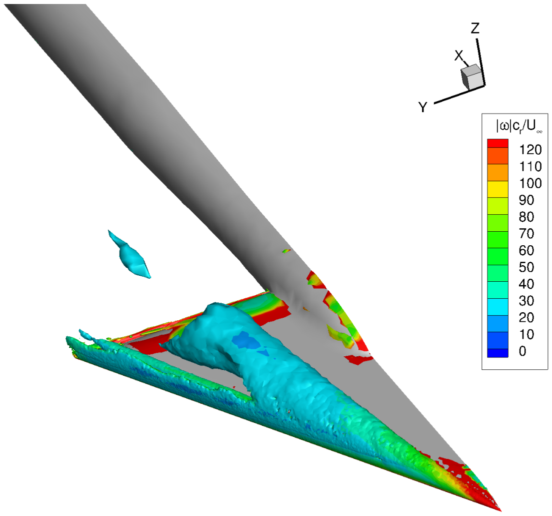

(a) Coarse Mesh

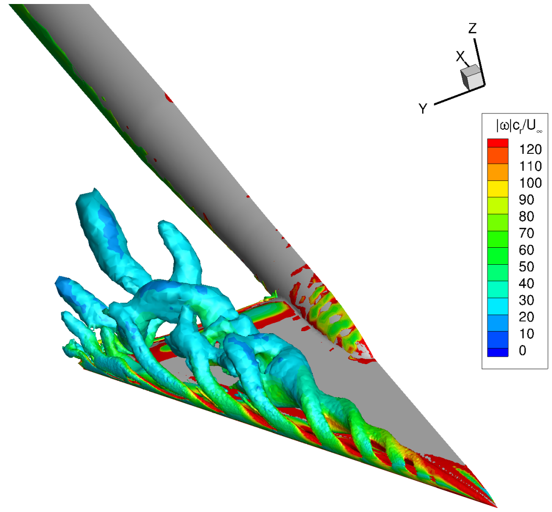

(b) Medium Mesh

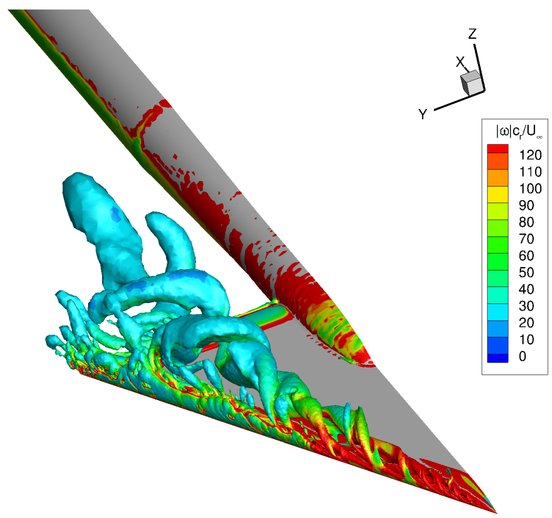

(c) Fine Mesh

Figure 6. Iso-surfaces of Q criterion colored by vorticity magnitude ($Q = 90U_\infty^2/c_r^2$)

References

[1]Chu, J. and Luckring, J. M. Experimental surface pressure data obtained on 65° delta wing across Reynolds number and Mach number ranges. *NASA TM 4645*, 1996.

[2]Breitsamter, C. and Furman, A. Turbulent and unsteady flow characteristics of delta wing vortex systems. *AIAA Paper 2008-0381*, 2008.

[3]Gursul, I. and Yang H. Vortex Breakdown Over a Pitching Delta Wing. *Journal of Fluids and Structures*, Vol. 9, Iss. 5, pp. 571 – 583, 1995.

[4]Morton, S. A., Forsythe, J. R., Mitchell, A. M., and Hajek, D. DES and RANS Simulations of Delta Wing Vortical Flows. *AIAA Paper 2007-1085*, 2007.

[5]Schiavetta, L. A., Badcock, K. J., and Cummings, R. M. Comparison of DES and URANS for unsteady vortical flows over delta wings *AIAA Paper 2002-0587*, 2002.

[6]Polhamus, E. C. A concept of the vortex lift of sharp edged delta wings based on a leading edge suction analogy. *NASA TN-3767*, 1966.

[7]Shur, M. L., Spalart, P. R., Strelets, M. Kh., Travin, A. Detached Eddy Simulation of an Airfoil at High Angle of Attack. *Engineering turbulence modelling and experiments* , 1999.

[8]Spalart, P. R., Deck, S., Shur, M. L., Squires, K. D., Strelets, M. Kh. and Travin, A. New Version of Detached-eddy Simulation, Resistant to Ambiguous Grid Densities. *Theoretical and Computational Fluid Dynamics*, Vol. 20, Iss. 3, pp. 181–195, 2006.

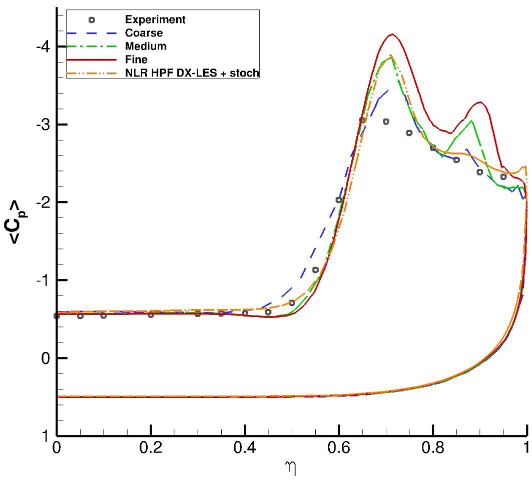

(a) $x/c_r = 0.20$

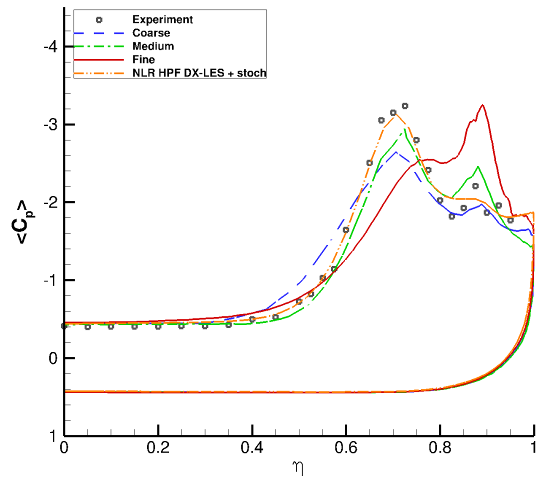

(b) $x/c_r = 0.40$

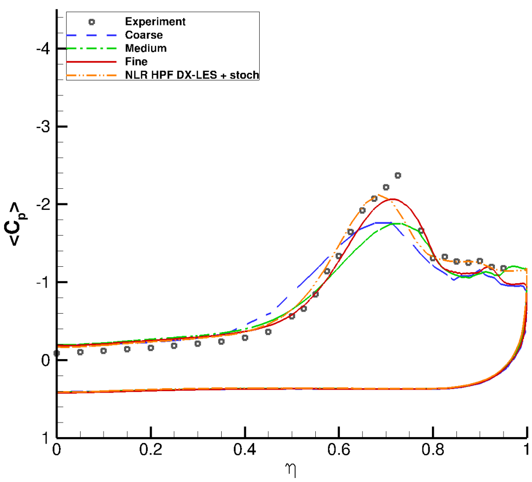

(c) $x/c_r = 0.60$

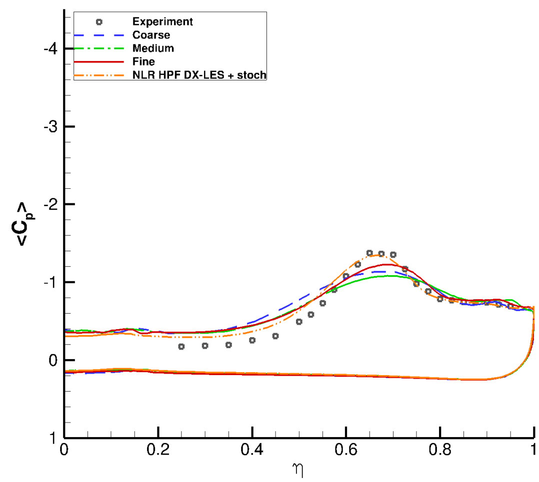

(d) $x/c_r = 0.80$

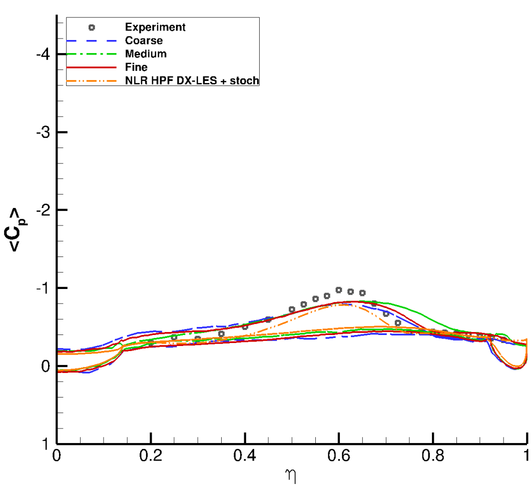

(e) $x/c_r = 0.95$

Figure 7. Mean pressure coefficient at 5 streamwise locations

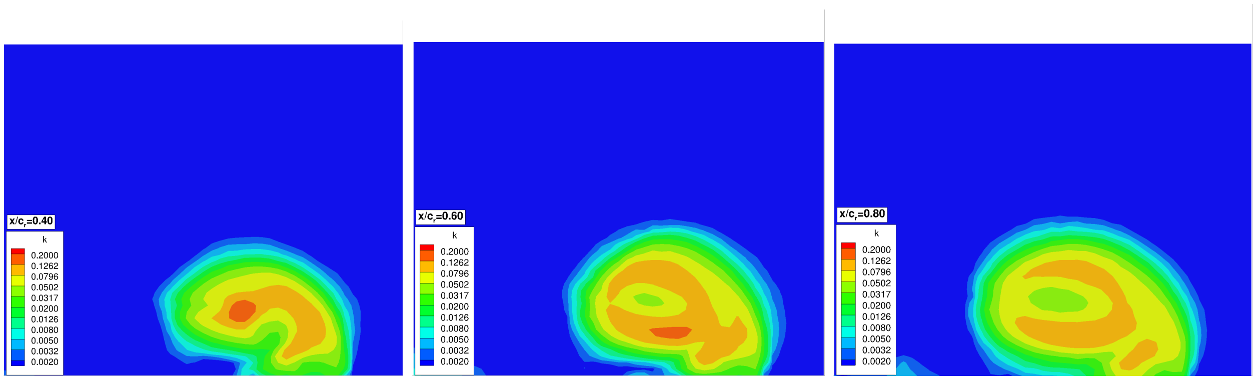

(a) Experiment, $x/c_r = 0.40$ (b) Experiment, $x/c_r = 0.60$ (c) Experiment, $x/c_r = 0.80$

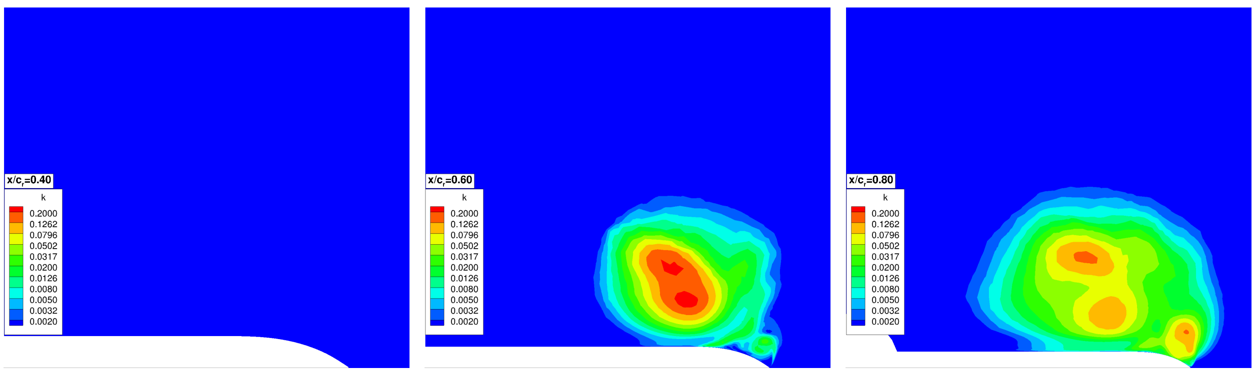

(d) Medium Mesh, $x/c_r = 0.40$ (e) Medium Mesh, $x/c_r = 0.60$ (f) Medium Mesh, $x/c_r = 0.80$

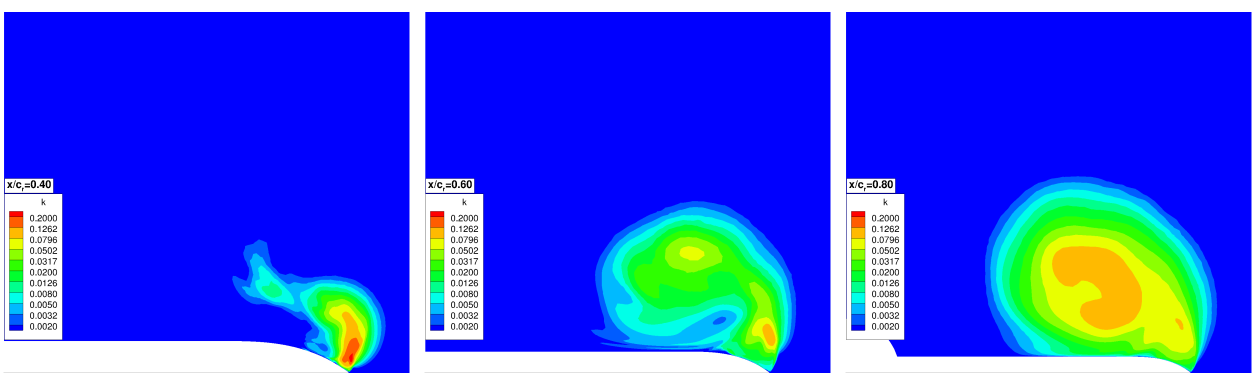

(g) Fine Mesh, $x/c_r = 0.40$ (h) Fine Mesh, $x/c_r = 0.60$ (i) Fine Mesh, $x/c_r = 0.80$

Figure 8. Measured and resolved turbulence kinetic energy at three streamwise locations. Top Row: Experiment; Middle Row: Medium Mesh; Bottom Row: Fine Mesh

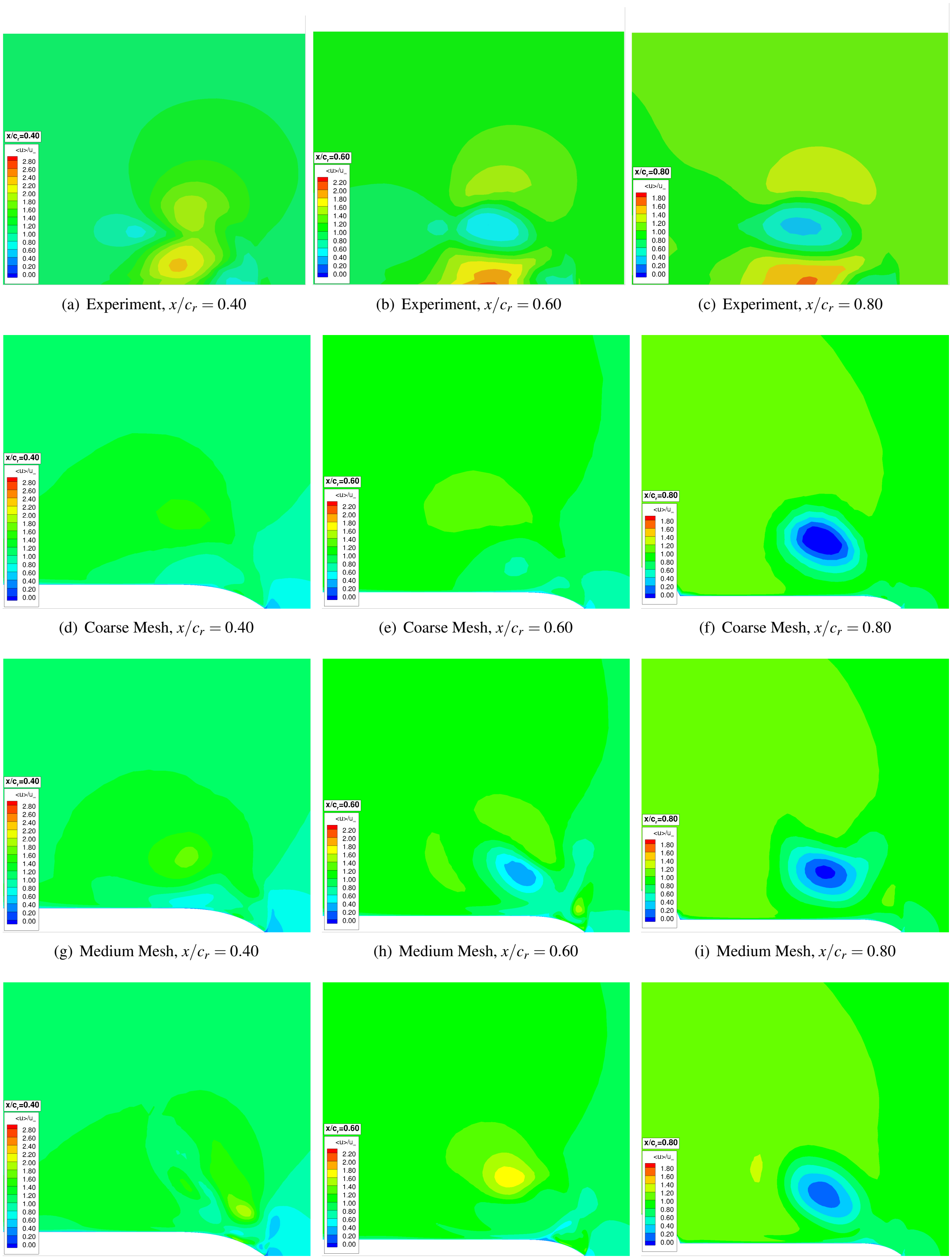

(a) Experiment, $x/c_r = 0.40$ (b) Experiment, $x/c_r = 0.60$ (c) Experiment, $x/c_r = 0.80$

(d) Coarse Mesh, $x/c_r = 0.40$ (e) Coarse Mesh, $x/c_r = 0.60$ (f) Coarse Mesh, $x/c_r = 0.80$

(g) Medium Mesh, $x/c_r = 0.40$ (h) Medium Mesh, $x/c_r = 0.60$ (i) Medium Mesh, $x/c_r = 0.80$

(j) Fine Mesh, $x/c_r = 0.40$ (k) Fine Mesh, $x/c_r = 0.60$ (l) Fine Mesh, $x/c_r = 0.80$

Figure 9. Mean streamwise velocity at three streamwise locations. Top Row: Experiment; Second Row: Coarse Mesh; Third Row: Medium Mesh; Bottom Row: Fine Mesh

[9]Spalart, P. and Allmaras, S. A one-equation turbulence model for aero- dynamic flows. *AIAA Paper 1992-0439*, 1992.

[10]Shur, M. L., Spalart, P. R., Strelets, M. Kh., Travin, A. An Enhanced Version of DES with Rapid Transition from RANS to LES in Separated Flows. *Flow, Turbulence and Combustion*, Vol. 95, Iss. 4, pp. 709–737, 2015.

[11]Pirzadeh, S. Vortical Flow Prediction Using an Adaptive Unstructured Grid Method. *Research & Technology Organization Applied Vehicle Technology Panel Meeting*, 2001

[12]Pardue, Juliette K and Chernikov, Andrey. Three-Dimensional Prism-Dominant Mesh Generation for Viscous Flows Around Surface Slope Discontinuities. *AIAA Paper 2018–3722*, 2018.

[13]Slotnick, J., Khodadoust, A., Alonso, J., Darmofal, D., Gropp, W., Lurie, E., and Mavriplis, D., CFD Vision 2030 Study: A Path to Revolutionary Computational Aerosciences. *NASA CR-2014-218178, Langley Research Center*, 2014.

[14]Park, Michael A. and Anderson, Kyle W. Spatial Convergence of Three Dimensional Turbulent Flows. *AIAA Paper 2016–859*, 2016.

[15]Ruppert, Jim. A Delaunay refinement algorithm for quality 2-dimensional mesh generation. *Elsevier, Journal of algorithms*, Vol. 18, Iss. 3, pp. 548–585, 1995.

[16]Shewchuk, Jonathan Richard. Triangle: Engineering a 2D quality mesh generator and Delaunay triangulator. *Springer, Applied computational geometry towards geometric engineering*, pp. 203–222, 1996.

[17]Drakopoulos, Fotis, Tsolakis, Christos and Chrisochoides, Nikos. Fine-Grained Speculative Topological Transformation Scheme for Local Reconnection Method *AIAA Paper 2018–2889*, 2018

[18]Drakopoulos, Fotis. Finite Element Modeling Driven by Health Care and Aerospace Applications. *Doctor of Philosophy (PhD), dissertation, Computer Science, Old Dominion University*, 2017

[19]Chrisochoides Nikos and Nave Démian. Parallel Delaunay Mesh Generation Kernel, *International Journal for Numerical Methods in Engineering*, Vol. 58, n. 2, pp. 161–176, 2003

[20]Foteinos Panagiotis and Chrisochoides Nikos . High Quality Real-Time Image-to-Mesh Conversion. *Journal on Parallel and Distributed Computing*, Vol. 74, n. 2, pp. 2123–21401, 2014

[21]Barth, Timothy. Numerical aspects of computing high Reynolds number flows on unstructured meshes. *29th Aerospace Sciences Meeting*, 1991

[22]Christos T., Chrisochoides N., Park, M. A., Loseille, A. and Michal T. R. Parallel Anisotropic Unstructured Grid Adaptation. *AIAA Paper 2019-1995* , 2019.

[23]Economon, T. D., Palacios, F., Copeland, S. R., Lukaczyk, T. W., Alonso, J. J. SU2: An Open-Source Suite for Multiphysics Simulation and Design, *AIAA Journal*, Vol. 54, n. 3, pp. 828–846, 2016

[24]Jameson, A. and Schenectady, S. An Assessment of Dual-Time Stepping, Time Spectral and Artificial Compressibility Based Numerical Algorithms for Unsteady Flow with Applications to Flapping Wings. *AIAA Paper 2009-4273*, 2009.

[25]Molina, E. S. Detached Eddy Simulation in SU2. *PhD Thesis, Aeronautical Institute of Technology*, 2018.

[26]Kitamura, K. and Hashimoto, A. Reduced dissipation AUSM-family fluxes: HR-SLAU2 and HR-AUSM+-up for high resolution unsteady flow simulations, *Computers & Fluids*, Vol. 126, pp. 41–57, 2016

[27]Kok, J. C. and van der Ven, H. Capturing free shear layers in hybrid RANS–LES simulations of separated flow. *Third Symposium 'Simulation of Wing and Nacelle Stall'*, 2012

[28]Saha, S. and Majumdar, B. Flow visualization and CFD simulation on 65° delta wing at subsonic condition. *Pocedia Engineering*, Vol. 38, pp. 3086–3096, 2012

[29]Kok, J., Fuchs, M. and Mockett, C. Delta Wing at High Angle of Attack. *Notes on Numerical Fluid Mechanics and Multidisciplinary Design*, pp. 139-153, 2018